ECCOMAS Congress 2016
VII European Congress on Computational Methods in Applied Sciences and Engineering
M. Papadrakakis, V. Papadopoulos, G. Stefanou, V. Plevris (eds.)
Crete Island, Greece, 5–10 June 2016

COMPARISON OF TETRAHEDRAL AND HEXAHEDRAL MESHES FOR FINITE ELEMENT SIMULATION OF CARDIAC ELECTRO-MECHANICS

Bernardo L. de Oliveira[1,2] **and Joakim Sundnes**[1,3]

[1]Simula Research Laboratory, Fornebu, Norway
[2]King's College London, London, United Kingdom
[3]University of Oslo, Oslo, Norway,
e-mail: bernardo.de_oliveira@kcl.ac.uk, sundnes@simula.no

Keywords: Cardiac Electro-mechanics, Finite Element Method.

Abstract. *The finite element method is an attractive method for solving the equations describing heart electrophysiology and mechanics. The finite element method with unstructured tetrahedral meshes is particularly suitable for representing complex geometrical shapes. On the other hand, hexahedral elements are generally thought to behave better for solid mechanics problems, and in particular for nearly incompressible, large-deformation hyperelasticity, which is normally encountered in the heart models. In this paper we compare the performance of tetrahedral and hexahedral elements for coupled electro-mechanics simulations, by running two different test cases chosen to represent different features of the coupled problem. A cuboid geometry was used to investigate the convergence of different elements for electrophysiology, while a truncated ellipsoid was used to assess the performance for active and passive mechanics. Both tests were run with linear and quadratic tetrahedral elements and with trilinear and triquadratic hexahedra. The results indicate that all four elements show very similar performance for the electrophysiology part of the problem, but linear tetrahedra stand out as the best choice. The differences are more substantial for the mechanics problem, where the linear tetrahedra showed severe mesh locking problems, and the trilinear hexahedra also performed poorly. The two quadratic elements behaved very similarly, with triquadratic hexahedra only slightly better. We may conclude based on these studies that quadratic tetrahedra are a suitable choice of element for coupled electro-mechanics simulations, which is convenient for image based modeling because of the large availability of automated meshing software.*

1 Introduction

Mathematical models of cardiac electro-mechanics are complex multiscale and multiphysics models consisting of coupled systems of ordinary and partial differential equations (ODEs and PDEs). The model components are typically systems of ODEs describing cellular dynamics and excitation-contraction coupling, a reaction-diffusion PDE describing tissue level electrophysiology, and a non-linear hyperelastic model describing the deformation of the tissue. The complete system is challenging to solve numerically, partly due to the overall complexity of the coupled system, and partly due to the properties of the model components. Specifically, the cell models ODEs are characterized by being stiff and strongly nonlinear, and more recent models consist of 50-100 equations. The reaction-diffusion equations based on bidomain or monodomain approximations require high resolution in space and time, because of rapid dynamics and steep gradients in the solution. Finally, the elasticity problem describing the mechanical deformations is characterized by strong nonlinearities, large deformations, strong anisotropy, and nearly incompressible material behavior. See, for instance, [1, 2, 3] for examples of solution approaches for the coupled system.

A variety of techniques have been used for cardiac electrophysiology, including the finite element (FE), finite difference (FD) and finite volume (FV) methods. For representing realistic heart geometries, FE and FV methods have an advantage over FD based schemes, as unstructured meshes based on tetrahedral elements are generally more convenient than structured meshes of hexahedra. The latter is due to the large availability of efficient automatic meshing tools for tetrahedral meshes [4], which facilitate constructing models based on medical images. A systematic comparison of electrophysiology solvers was presented by Niederer et al. [5], and further discussed and explored in subsequent studies [6, 7]. These studies discuss the different characteristics of FE and FD methods, and the effect of solver choices such as operator splitting schemes and mass lumping, but do not discuss the numerical properties of different element types. Although a number of different element types have been used and reported in the literature, their performance for solving the bidomain or monodomain equations has not been systematically compared.

For solid mechanics problems, and for coupled cardiac electro-mechanics in particular, FE methods are the dominating scheme for spatial discretization. Furthermore, there is a general agreement that for solid mechanics and structural engineering problems, hexahedral elements present better accuracy and efficiency than tetrahedral elements, in particular for low order elements [8]. Due to the higher inherent stiffness of tetrahedral elements, they require higher strain energy states to deform than hexahedral elements [9], and are associated with problems of mesh locking [10]. This phenomenon causes exaggerated errors in the solutions due to the inability of the finite element interpolation functions to correctly approximate volume preserving strain fields [11].

Benzley et al. [9] compared how different elements perform for various elastic and elasto-plastic problems. For elastic problems, linear tetrahedra (LT) produced unacceptably high errors. Trilinear hexahedra (LH) provided acceptable results but required significant refinement in certain cases and both quadratic tetrahedra (QT) and triquadratic hexahedra (QH) provided adequate results in all problems. On the elasto-plastic calculations, again LT produced unacceptable errors and QH produced the best results. However, LH produced results superior to QT.

Different studies have examined how tetrahedra and hexahedra perform when modeling biological tissues. Ramos and Simes [12] studied how the different elements perform to model

the proximal femur in a linear elasticity framework. For a simplified test case they found that LT better approximated the theoretical solution. On a more complex and realistic test case no significant difference were observed between the different elements solutions. A similar comparison, more closely related to the heart mechanics problem, was made by Tadepalli et al. [13] in a problem of foot biomechanics. This problem presents material nonlinearities, incompressibility and large deformations. They concluded that hexahedral elements consistently produced reasonable pressures and stresses, while linear tetrahedral elements only produced reasonable results when the incompressibility could be relaxed.

The purpose of this work is to study the convergence characteristics and performance of different types of elements for cardiac mechanics and electrophysiology. More specifically, we want to investigate the suitability of tetrahedral meshes for cardiac mechanics, and study the performance of linear and quadratic elements for both electrophysiology and mechanics. The paper is organized as follows. In Section 2 we give a detailed presentation of the mathematical problem, and of the test cases used to compare element performance. Results of the numerical experiments are then presented in Section 3, and their implications and limitations are discussed in Section 4. Finally, in Section 5 we present conclusions and recommendations regarding suitable element types for electrophysiology, mechanics, and coupled electro-mechanics problems.

2 Models and methods

2.1 Mathematical Models

Models for cardiac electromechanics can be formulated as coupled systems of ODEs and PDEs. In this work the monodomain model was adopted for the electrophysiology, while the tissue mechanics was described with a hyperelastic model. The main equations of the model read

$$\frac{\partial \mathbf{s}}{\partial t} = f(v, \mathbf{s}, \lambda), \tag{1}$$

$$\chi \left(C_m \frac{\partial v}{\partial t} + I_{ion}(v, \mathbf{s}, \lambda) \right) = \nabla \cdot (\mathbf{D} \nabla v), \tag{2}$$

$$\nabla \cdot (\mathbf{F}\mathbf{S}) = 0, \tag{3}$$

with the constitutive relations

$$\mathbf{S} = \mathbf{S}^p + \mathbf{S}^a \tag{4}$$

$$\mathbf{S}^a = J\mathbf{F}^{-1}\sigma^{\mathbf{a}}(\mathbf{s}, \lambda, \dot{\lambda})\mathbf{F}^{-T} \tag{5}$$

$$\mathbf{S}^p = \frac{\partial \Psi}{\partial \mathbf{E}} \tag{6}$$

$$\Psi = \frac{1}{2}C(e^W - 1) + C_{compr}(J \ln J - J + 1) \tag{7}$$

$$W = b_{ff}E_{ff}^2 + b_{xx}(E_{ss}^2 + E_{nn}^2 + E_{sn}^2 + E_{ns}^2) + b_{fx}(E_{fn}^2 + E_{nf}^2 + E_{fs}^2 + E_{sf}^2). \tag{8}$$

and the boundary conditions

$$\mathbf{n} \cdot (\mathbf{M}\nabla v) = 0, \qquad \mathbf{x} \in \partial H(t), \tag{9}$$

$$\mathbf{u} = 0, \qquad \mathbf{x} \in \partial H_1(0), \tag{10}$$

$$\mathbf{T} = J\bar{\sigma}_1 \mathbf{F}^{-T} \cdot \eta, \ \mathbf{x} \in \partial H_2(0), \tag{11}$$

$$\mathbf{T} = J\bar{\sigma}_2(t) \mathbf{F}^{-T} \cdot \eta, \ \mathbf{x} \in \partial H_3(0). \tag{12}$$

Here, (1) is a system of ODEs describing cell dynamics, including cell electrophysiology and excitation-contraction coupling. The cell state is characterized by the vector $\mathbf{s}$, v is the membrane potential, and λ is fiber stretch. The fiber stretch is calculated from the Green-Lagrange strain tensor $\mathbf{E}$, as $\lambda = \sqrt{2E_{ff} + 1}$, with f indicating the local fiber direction. In this work two different electrophysiology cell models were used, one by ten Tusscher et al [14] and and one from Winslow et al [15]. These models were coupled to the myofilament model by Rice et al [16]. More details on the coupling can be found in [3, 17]. Eq. (2) is the monodomain model, which describes electrical signal conduction through the tissue. Here χ is the ratio of cell membrane area to tissue volume, C_m is cell membrane capacitance, D is tissue conductivity and I_{ion} is the transmembrane current. A no-flux boundary condition is employed, see (9), where $\mathbf{n}$ is the unit surface normal of the deformed heart surface.

The mechanics of the heart muscle is described by the equilibrium equation (3), combined with the constitutive relations (4)-(8). Here, $\mathbf{F}$ is the deformation gradient, $\mathbf{S}$ is the second Piola-Kirchhoff stress tensor, and $E_{ij}, i, j = f, s, n$ are components of the Green-Lagrange strain tensor $\mathbf{E} = 1/2(\mathbf{F}^T\mathbf{F} - 1)$. Eq. (4) describes an additive decomposition of the stress tensor into a passive part $\mathbf{S}^p$ and an active part $\mathbf{S}^a$. The passive component $\mathbf{S}^p$ is derived from the strain-energy density (7)-(8) [18], where C, b_{ff}, b_{xx} and b_{fx} are material parameters. The material is considered almost incompressible, with C_{compr} being a penalty factor used to control volume changes, and J the determinant of $\mathbf{F}$. The active stress component is calculated by mapping the active Cauchy stress tensor, $\sigma^{\mathbf{a}}$, to the reference configuration, as in (5). In local fiber coordinates we have $\sigma^{\mathbf{a}} = \text{diag}(T_a, \eta T_a, \eta T_a)$, where η is a constant and $T_a(\mathbf{s})$ is the dynamic tension computed from the cell model state vector. The subscripts f, s and n correspond to the fiber, sheet and sheet-normal directions, respectively. The mechanics boundary conditions are given by (10)-(12), where $\mathbf{u}$ is displacement, $\bar{\sigma}_1, \bar{\sigma}_2$ are prescribed stresses on the heart surface, and η is the unit surface normal of the undeformed reference geometry.

2.2 Numerical Methods

A common approach to solve (1)-(8) is to apply an operator splitting technique to divide the system into smaller sub-problems. Here, we have used the splitting method from [3], where the mechanics problem is separated from the electrophysiology part by means of a Gauss-Seidel approach, and a Godunov splitting is applied to (2) to separate the nonlinear reaction term from the diffusion part. Three separate problems must be solved for each time step; a nonlinear system of ordinary differential equations describing cell electrophysiology and force generation, a linear parabolic PDE that represents the electro-diffusion in the cardiac tissue, and a nonlinear elasticity equation describing the mechanical deformations. Assuming that the variables v_n, $\mathbf{s}_n$ and $\mathbf{u}_n$ are known at time t_n, the solution is advanced by the following procedure:

1. Solve the nonlinear ODE system

$$\frac{dv}{dt} = -I_{ion}(v, s, \lambda_n), \qquad t_n < t < t_{n+1}, v(t_n) = v_n, \tag{13}$$

$$\frac{ds}{dt} = f(v, s, \lambda_n), \qquad t_n < t < t_{n+1}, s(t_n) = s_n. \tag{14}$$

An updated vector s_{n+1} is obtained, together with an intermediate updated transmembrane potential v^*. Note that the fiber stretch is held constant over this integration step, $\lambda = \lambda_n$ [19]. This system of ODEs was solve using a third-order Singly Diagonally Implicit Runge-Kutta method with adaptive time stepping, see [20].

2. Solve the parabolic linear PDE using v^* as the initial condition,

$$\nabla \cdot (\mathbf{D}\nabla v) = \frac{\partial v}{\partial t} \tag{15}$$

Our strategy to solve this equation is to discretize it in time using a backward Euler scheme:

$$\nabla \cdot (\mathbf{D}\nabla v^{n+1}) = \frac{v^{n+1} - v^*}{\Delta t} \tag{16}$$

For spatial discretization of (16), we apply a standard Galerkin FE formulation. In short, for a suitable function space $\Phi(\Omega)$, we multiply both sides of (16) with a test function $\phi \in \Phi(\Omega)$, and integrate over the domain Ω. Integration by parts and application of the homogeneous Neumann boundary condition leads to the following weak form:
Find $v^{n+1} \in \Phi(\Omega)$ such that:

$$\int_\Omega v^{n+1}\phi d\Omega + \Delta t \int_\Omega \mathbf{D}\nabla v^{n+1}\nabla\phi d\Omega = \int_\Omega v^*\phi d\Omega, \quad \forall \phi \in \Phi(\Omega) \tag{17}$$

This variational problem is discretized by defining a finite-dimensional subspace $\Phi_h(\Omega) \subset \Phi(\Omega)$, and approximating the solution as a linear combination of the basis functions of Φ_h; $v = \sum_i v_i, \phi_i$. This standard FEM procedure leads to a linear system that is solved using a multigrid preconditioned conjugate gradient method, see e.g. [19] for details.

3. Solve the nonlinear mechanics problem using the most recently calculated value of the state vector , s^{n+1}, to calculate the active stress tensor $\mathbf{S}^a$

$$\nabla \cdot \Big(\mathbf{F}(\mathbf{S}^p + \mathbf{S}^a(s^{n+1}, \lambda, \dot{\lambda}))\Big) = 0 \tag{18}$$

The mechanical problem is solved by a standard, displacement-based Galerkin FEM. Applying similar steps as for the diffusion problem above leads to a system of non-linear algebraic equations to be solved for the unknown displacement field. We solve this system iteratively by the Newton-Raphson method, which involves a linearization of all relevant quantities. For each iteration of the Newton-Raphson method, we solve a linear system with the stiffness matrix

$$A_{ij} = \int_\Omega \nabla\phi_i : \mathcal{A} : \nabla\phi_j d\Omega, \tag{19}$$

where $\mathcal{A}$ is the first elasticity tensor, which characterizes the tangential stiffness of the tissue. See for instance [21, 22] for details on the displacement-based FE formulation for large elastic deformations. Following the additive split in (4), the fourth-order tensor $\mathcal{A}$ has contributions from the active and passive strain components,

$$\mathcal{A}_{ijkl} = \frac{\partial\{\mathbf{F}\mathbf{S}^{\mathbf{p}}\}_{ij}}{\partial\mathbf{F}_{kl}} + \frac{\partial\{\mathbf{F}\mathbf{S}^{\mathbf{a}}\}_{ij}}{\partial\mathbf{F}_{kl}}. \tag{20}$$

Both terms are computed by numerical differentiation of the stress-strain relation. The passive part the stress-strain relation is obtained by analytical differentiation of the strain energy function in (6), while the active part is obtained by a pull-back of the active Cauchy stress, as defined in (5).

2.3 Test Cases

A key challenge in defining the test cases to compare the different element types is to decide the level of complexity that should be adopted. On one hand, it is interesting to keep the tests simple so they can be clearly expressed, take a limited amount of time and computational resources to be performed and can be more easily communicated and reproduced. On the other hand, the test cases must be complex enough to be physiologically relevant and unravel the performance characteristics of the methods when applied to more realistic and complex simulations. Two different test cases are considered in this study.

The first test case only considers electrophysiology, and is inspired by Niederer et al. [5], where different electrophysiology simulators were tested, and the results were compared in terms of the conduction velocity. We adopted the same simplified geometry and stimulation protocol. A rectangular box of dimensions 3 x 7 x 20 mm^3 was used, with fibers aligned in the longer axis. Regular grids were generated for this geometry using different element types and node spacing. The fiber conductivity was set to 1.33 mS cm^{-1}, the transversal conductivity was 0.18 mS cm^{-1} and the surface to volume ratio was 1400 cm^{-1}. A stimulation current was applied in one corner, point P1 in Figure 1. These tests were performed using two different cell models. A zero flux boundary condition was assumed implicitly in the whole boundary. The quality of the solutions was measured similarly to Niederer et al. [5], by comparing the activation times of the last node in the mesh, point P2 on Figure 1. This activation time can be used to get a good estimative of the conduction velocities of the electrical signal, which is known to be highly sensitive to the mesh resolution. As disturbances in the conduction velocity are often associated with arrhythmias and other pathologies it is of great importance to have converged conduction velocities in order to support any physiological or clinical conclusions based on electrophysiological simulations.

The second test case is focused on active and passive mechanics. The geometry is a truncated ellipsoid as shown in Figure 2, which is a reasonable approximation of a left ventricle. The fiber field was set as aligned in the tangential direction of the geometry, with a rotation from -30^o to 30^o from epicardium to endocardium. Although we ran the full coupled model, (1)-(8), electrical activation was applied homogeneously and simultaneously to the entire domain. Effects of electrical diffusion are therefore minimized, and the main focus is on the mechanics. The material parameters C, b_{ff}, b_{xx} and b_{fx} were chosen to be 0.25 kPa, 50, 25 and 25 respectively. The incompressibility penalty factor C_{compr} was chosen to be 200 kPa. This choice gave the realistic nearly incompressible behavior of the myocardium, with volume changes ¡5%, which is known to lead to mesh locking that will highlight the difference between element types.

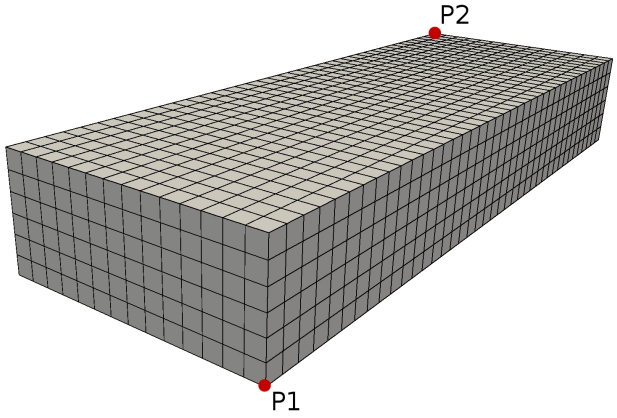

Figure 1: A rectangular box geometry taken from [5] was used for the pure electrophysiology comparison.

For boundary conditions, the base was fixed in the longitudinal direction, and two additional points on the base were constrained to avoid rigid body movement. The outer (epicardial) surface was assumed stress-free, while a time-varying pressure was applied to the endocardium, to capture the four phases of a generic pressure-volume (PV) loop. Each test would start with the passive filling phase, where the endocardial pressure was increased from 0 to 2 kPa over a time interval of 200 ms. At $t = 180$ms, stimulus was applied to trigger contraction, and a simplified circulation model was used for the remaining phases of the heart cycle. The following equations were solved to determine the endocardial pressure:

$$\frac{dV_{cav}}{dt} = -q_{ao}, \tag{21}$$

$$q_{ao} = \max(C_{art}\frac{dp}{dt} + R_{per}(p - p_{per}), 0). \tag{22}$$

Here V_{cav} is the cavity volume computed from the deformed FEM mesh, q_{ao} is the aortic flow, p is the cavity pressure applied to the endocardial boundary, C_{art} is the compliance of the systemic arterial tree, R_{per} is peripheral resistance and p_{per} is the peripheral pressure. By inserting (22) into (21) and applying a finite difference approximation for the time derivative, we get a non-linear equation which can solved for the cavity pressure p by an iterative Newton algorithm, see e.g. [3] for details.

3 Results

3.1 Electrophysiology

Several simulations were performed using meshes with different resolutions and element types. The coarsest mesh had 4305 degrees of freedom (DOFs), which corresponds to a node spacing of 0.5 mm. Four levels of refinement were used, with each level reducing the node spacing by a factor of two, which corresponds to a factor eight increase in the number of DOFs. Due to limitations in our software the last level of refinement could not be simulated with QTs. Since the PDE is discretized in both time and space, results from two different time stepping values, 50μs and 10μs, are presented to investigate how the error introduced by the time discretization affect the results.

The activation times obtained in the simulations can be seen on Figure 3. The top row shows the results from the model by ten Tusscher et al., and the bottom row shows results of

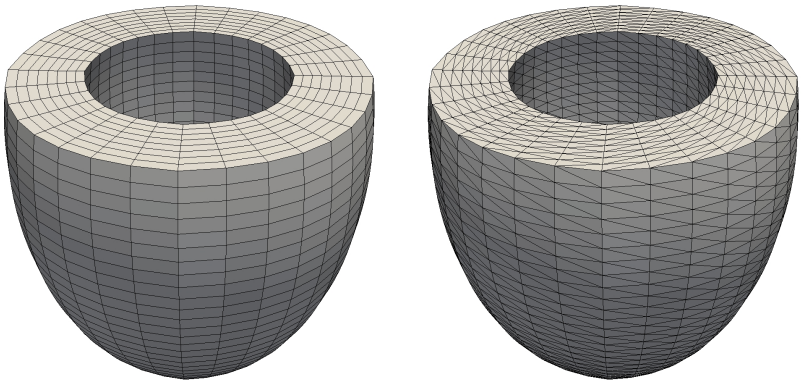

Figure 2: An ellipsoidal geometry was used for the mechanical test cases with hexahedra and tetrahedra

the Winslow et al. model. We observed signal conduction in all levels of refinement with the ten Tusscher et al model, while the model by Winslow et al did not conduct on the coarsest meshes. The results displayed in the bottom row therefore starts at one level of refinement. The conduction block can be explained by the lower upstroke velocity of the Winslow et al model, which leads to a lower conduction velocity and increased risk of conduction block. We see that the LT elements consistently give lower activation time (higher conduction velocity) than the other elements, but there are no substantial differences between the element types. All elements produce unacceptable errors on the coarsest meshes, while on the fourth level of refinement all solutions are visually very similar. Note also that the difference between the two time step values is larger for the model by ten Tusscher et al. The larger time discretization errors seen for this model can be explained by the higher upstroke velocity.

The relative errors in the activation times are shown in Figure 4. Since no analytical solution is available, we calculated the reference activation time as the average of the computations on the finest grid, with a time step of 10μs and a node spacing of 62.5μm. While this choice of reference will clearly not give accurate errors for the finer meshes, it does provide a useful measure for comparing the coarsest meshes. The error plots show a similar behavior as the previous plots, with relatively small differences between the element types. The slightly less consistent results can be explained by the shape of the curves in Figure 3, which show that all the elements overestimate the activation time (i.e. underestimate the conduction velocity) on the coarse meshes, but as the mesh is refined further most elements underestimate the time and approach the correct value from below. This behavior, which can be shown analytically for simplified models, means that a fairly coarse mesh may give a very accurate conduction velocity, and that the error may increase as the grid is refined. The error from time discretization is also very visible in the upper left corner, which shows all the curves converging to a value significantly different from the reference.

3.2 Mechanics

For this test case, again, the solutions using meshes with different levels of refinement and elements were compared. The coarsest mesh had 219 degrees of freedom (DOFs). Three levels of refinement were used, with each level increasing the number of DOFs by a factor of eight. As for the electrophysiology problem, no analytical solution is available. Instead, we compute a reference solution by running one simulation with an additional level of refinement.

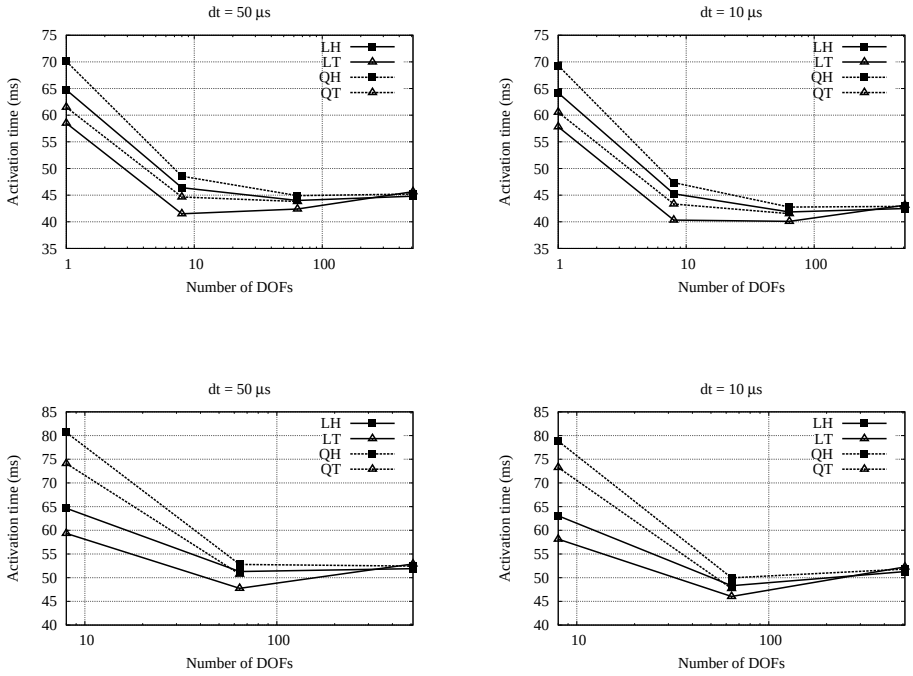

Figure 3: Activation times with the ten Tusscher (top) and Winslow (bottom) models. The number of DOFs is normalized by the coarsest mesh.

We first compared the elements for the passive inflation phase, by computing the relative error in displacement and stress. The left panel of Figure 5 shows the L2 error norm of the displacement fields. We see that for this problem the quadratic elements outperform the linear ones, and the LT elements are particularly bad, producing unacceptable errors for all refinement levels. This result is in line with previous results and with the general view of the solid mechanics community, that LT are not suited for nearly incompressible elasticity problems. However, QH and QT elements show very similar behavior, indicating that the poor performance of tetrahedra is limited to linear elements. The right panel of Figure 5 shows the L2 error norm of the stress fields. These results show an even clearer advantage of quadratic elements, as both the linear elements produce large errors. However, the difference between QH and QT is only significant on the coarser meshes.

To further investigate the performance of the different element types, we computed the full PV loops, shown in Figure 3.2. The PV loops were computed as specified in Section 2, by first ramping up the pressure to a specified end diastolic pressure, and then solve (21)-(22) for the isovolumic and ejection phases. The top left panel shows results for the coarsest mesh, the top right panel is for one level of refinement, while the bottom panel shows the finest mesh. We can see that for the coarsest mesh, both the linear elements show a much higher stiffness than the quadratic ones, and inflate to lower end diastolic volumes. The two quadratic elements show very similar behavior even for this coarse mesh. On the second level of refinement the curves for the two quadratic elements visually overlap. The linear elements also show much better results on this level, although the end diastolic volume is still significantly lower than the reference. On the third level of refinement all curves are visually very similar.

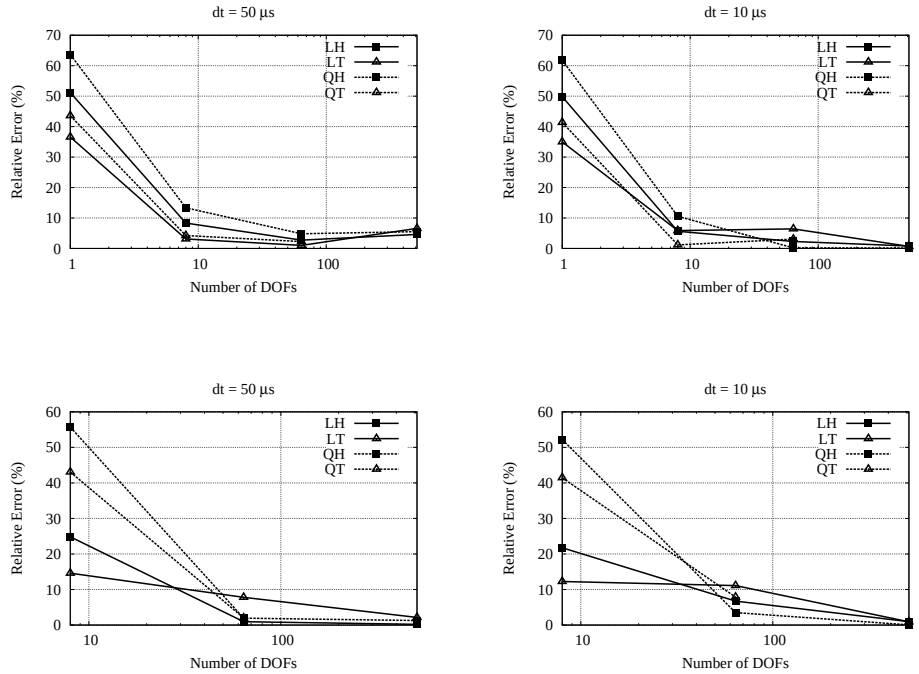

Figure 4: Relative error of the activation times with the ten Tusscher(top) and Winslow (bottom) models. The number of DOFs is normalized by the coarsest mesh.

4 Discussion

We have compared different element types for simulations of cardiac electrophysiology and mechanics, with the aim of testing the common conception that hexahedral elements are superior to tetrahedra for solid mechanics applications, and to compare the elements' performance for coupled simulations.

For the test case involving pure electrophysiology, no firm conclusions could be made regarding the suitability of different element types. All element types produced unacceptable errors for the coarsest mesh, and also for one level of refinement. On the second level of refinement, with node spacing of 250 μm, most of the results were within 5 to 10% from the reference activation time. These errors are normally considered too large for practical applications. For a node spacing of 62.5 μm, the variation between solutions is less than 1%. However, the com-

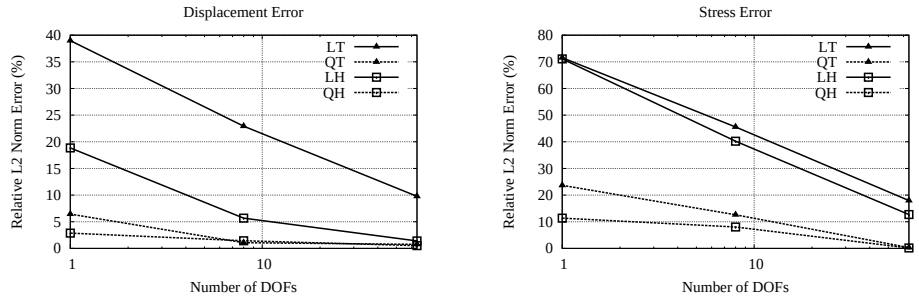

Figure 5: L2 Error of the displacement (left) and stress (right).

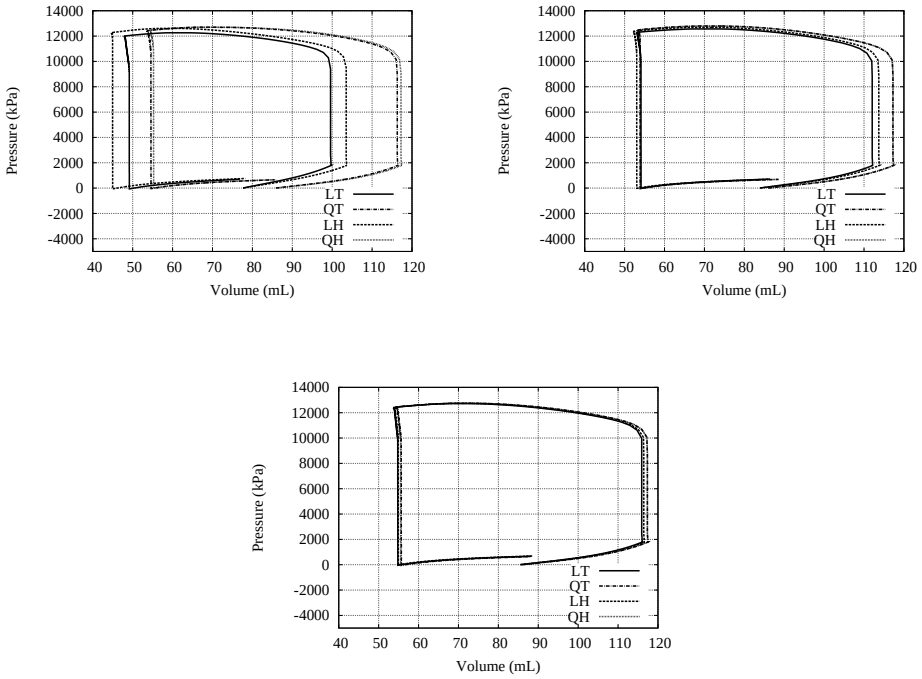

Figure 6: PV loops for the four different element types and three levels of refinement. The top left is the coarsest mesh, top right is for one level of refinement, and the bottom panel is the finest mesh.

parison made here is entirely based on comparing the error for a given number of degrees of freedom, not looking at the actual CPU time for each element type. The CPU time per degree of freedom is higher for quadratic than for linear elements, and one may argue that our results indicate that linear elements perform better. For some cases, the CPU time for QH and QT was up to 30% higher than for LH and LT, resulting from increased cost of assembling and solving the linear systems.

The mechanics cases show a clear advantage of quadratic elements, which is in line with previous results in the literature, see, e.g. [9], and what seems to be the general opinion in the field. However, the difference between hexahedra and tetrahedra was somewhat smaller than expected. For passive inflation, LH clearly outperformed LT, but they both showed large errors, in particular when comparing the stress fields. The QH elements proved superior to QT, but the differences are small. The simulations of full PV loops confirmed the results from the passive inflation case, in that the linear elements substantially overestimated the overall stiffness of the ventricle. However, when comparing the plots in Figure 3.2 to the displacements in Figure 5, the PV loops seem to be more converged than the displacements for the second grid level, which has an average node spacing of 0.75cm. A more careful examination reveals that this apparent discrepancy is due to linear elements better capturing the radial displacement than the shear strains and torsion of the ellipsoid. This inability of the linear elements, particularly the tetrahedra, to capture the shear strains observed in the reference solution are a strong indication of the phenomenon of mesh locking [10].

There are a number of limitations to the present study, some of which are natural candidates for future research. Our study has focused on a limited selection of element types, and considering two relatively simple model problems. However, the elements considered herein are widely used in the cardiac modeling community, and are among the most widely available ele-

ment types in automatic meshing software. For an even more representative element selection it would be useful to include elements based on cubic Hermite interpolation, as these are common for cardiac modeling, see e.g. [18]. However, Hermite elements were not available in the FE frameworks available for this study, and adding these elements to the frameworks is a considerable task which has been left for future investigations. Other limitations include the simplicity of the two test cases. These were chosen to be representative of more advanced simulation models, but still be sufficiently simple to enable a rudimentary convergence study. Furthermore, although the final test case is a fully coupled simulation, the effects of electro-diffusion are negligible because of the simultaneous activation pattern. A fully coupled simulation with a propagating signal may give additional results, but will also considerably complicate the analysis, since the meshes considered here are too coarse for conduction of the electrical signal.

5 Conclusions

Any conclusions on element choice are naturally affected by the available software and choice of solution method. The operator splitting technique employed in this study is representative for a number of solution methods applied in the field, and enables a decoupled solution of the mechanics and electrophysiology sub-problems. However, even with this uncoupling, it is convenient to work with nested meshes, where the electrophysiology mesh is a refinement of the mechanics mesh. This consideration motivates the use of identical or similar elements for the two problems. It is possible to implement a more general operator splitting scheme, where the meshes and elements for electrophysiology and mechanics are completely independent, as well as more tightly coupled schemes that employ identical meshes for the two sub-problems. These solver choices will obviously affect the choice of elements, but results presented here are representative for a widely used class of solution scheme.

The main conclusion of this work is that quadratic and triquadratic elements are best suited for coupled electro-mechanics. These elements show superior performance for mechanics, and comparable performance as the linear elements for the electrophysiology part. For pure electrophysiology simulations, our results indicate that LT elements should be chosen, but this should always be avoided for mechanics computations. No significant difference is seen between QH and QT elements, which indicates that the added geometric flexibility of tetrahedral meshes make them highly attractive for image based and patient specific modeling.

REFERENCES

[1] S. A. Niederer and N. P. Smith. An improved numerical method for strong coupling of excitation and contraction models in the heart. *Prog Biophys Mol Biol*, 96:90–111, 2008.

[2] Serdar Göktepe and Ellen Kuhl. Electromechanics of the heart: a unified approach to the strongly coupled excitation–contraction problem. *Computational Mechanics*, 45(2-3):227–243, November 2009.

[3] J. Sundnes, S. Wall, H. Osnes, T. Thorvaldsen, and A.D. McCulloch. Improved discretisation and linearisation of active tension in strongly coupled cardiac electro-mechanics simulations. *Computer Methods in Biomechanics and Biomedical Engineering*, 17:604–615, 2014.

[4] Hang Si. Tetgen: A quality tetrahedral mesh generator and a 3d delaunay triangulator. url: http://wias-berlin.de/software/tetgen/, June 2014.

[5] Steven A. Niederer, Eric Kerfoot, Alan P. Benson, Miguel O. Bernabeu, Olivier Bernus, Chris Bradley, Elizabeth M. Cherry, Richard Clayton, Flavio H. Fenton, Alan Garny, Elvio Heidenreich, Sander Land, Mary Maleckar, Pras Pathmanathan, Gernot Plank, Jos F. Rodrguez, Ishani Roy, Frank B. Sachse, Gunnar Seemann, Ola Skavhaug, and Nic P. Smith. Verification of cardiac tissue electrophysiology simulators using an n-version benchmark. *Philosophical Transactions of the Royal Society A*, 369:43314351, 2011.

[6] P. Pathmanathan, M.O.Bernabeu, S.A.Niederer, D.J.Gavaghan, and D. Kay. Computational modelling of cardiac electrophysiology: explanation of the variability of results from different numerical solvers. *International Journal for Numerical Methods in Biomedical Engineering*, 28:890–930, 2012.

[7] Shankarjee Krishnamoorthi, Mainak Sarkar, and William S. Klug. Numerical quadrature and operator splitting in finite element methods for cardiac electrophysiology. *International Journal for Numerical Methods in Biomedical Engineering*, 29:1243–1266, 2013.

[8] John R. Brauer. *What Every Engineer Should Know About Finite Element Analysis*. Marcel Dekker Inc, 1993.

[9] Steven E. Benzley, Ernest Perry, Karl Merkley, Brett Clark, and Greg Sjaardema. A comparison of all hexagonal and all tetrahedral finite element meshes for elastic and elastoplastic analysis. In *In Proceedings, 4th International Meshing Roundtable*, 1995.

[10] Thomas J.R. Hughes. *The Finite Element Method: Linear Static and Dynamic Finite Element Analysis*. Englewood Cliffs, 1987.

[11] Allan F. Bower. *Applied Mechanics of Solids*. CRC Press, 2009.

[12] A. Ramos and J.A. Simes. Tetrahedral versus hexahedral finite elements in numerical modelling of the proximal femur. *Medical Engineering and Physics*, 28:916924, 2006.

[13] Srinivas C. Tadepalli, Ahmet Erdemir, and Peter R. Cavanagh. Comparison of hexahedral and tetrahedral elements in finite element analysis of the foot and footwear. *Journal of Biomechanics*, 44:23372343, 2011.

[14] K. H. ten Tusscher, D. Noble, P. J. Noble, and A. V. Panfilov. A model for human ventricular tissue. *Am J Physiol Heart Circ Physiol*, 286:1573–1589, 2004.

[15] Raimond L. Winslow, Jeremy Rice, Saleet Jafri, Eduardo Marbn, and Brian ORourke. Mechanisms of altered excitation-contraction coupling in canine tachycardia-induced heart failure, ii model studies. *Circulation Research*, 84:571–586, 1999.

[16] J. Rice, F. Wang, D. Bers, and P. Tombe. Aproximate model of cooperative activation and crossbridge cycling in cardiac muscle using ordinary differential equations. *Biophysical Journal*, 95:2368–2390, 2008.

[17] B. L. de Oliveira, B. M. Rocha, L. P. S. Barra, E. M. Toledo J. Sundnes, and R. Weber dos Santos. Effects of deformation on transmural dispersion of repolarization using in silico models of human left ventricular wedge. *International Journal for Numerical Methods in Biomedical Engineering*, 29:13231337, 2013.

[18] Taras P. Usyk, Ian J. LeGrice, and Andrew D. McCulloch. Computational model of three-dimensional cardiac electromechanics. *Computing and Visualization in Science*, 4:249–257, 2002.

[19] J. Sundnes, G. T. Lines, and A. Tveito. An operator splitting method for solving the bidomain equations coupled to a volume conductor model for the torso. *Mathematical Biosciences*, 194:233–248, 2005.

[20] J. Sundnes, G. Lines, and A. Tveito. Efficient solution of ordinary differential equations modeling electrical activity in cardiac cells. *Mathematical Biosciences*, 172:55–72, 2001.

[21] G A Holzapfel. *Nonlinear solid mechanics: a continuum approach for engineering*. Wiley, 2000.

[22] J. Bonet and R.D. Wood. *Nonlinear continuum mechanics for finite element analysis*. Cambridge University Press, 1997.